# ANALYSIS OF THE R FAMILY OF LIMITERS APPLIED TO HIGH-ORDER FR/CPR SCHEMES FOR THE SIMULATION OF SUPERSONIC FLOWS

Frederico Bolsoni Oliveira<sup>1</sup>, João Luiz F. Azevedo<sup>2</sup> & Z. J. Wang<sup>3</sup>

<sup>1</sup>Instituto Tecnológico de Aeronáutica, São José dos Campos, São Paulo 12228-900, Brazil
 <sup>2</sup>Instituto de Aeronáutica e Espaço, São José dos Campos, São Paulo 12228-904, Brazil
 <sup>3</sup>University of Kansas, Lawrence, Kansas 66045, USA

# **Abstract**

The present investigation assesses a novel family of flux limiter formulations to be used with high-order flux reconstruction or correction procedure via reconstruction (FR/CPR) schemes to simulate supersonic flows typical of aerospace applications. A modification to the original formulation is also presented such that unwanted limiter activations in smooth regions of the flow are reduced. Solutions obtained with such limiters are compared to other well-established formulations currently available in the literature by employing a two-dimensional, inviscid, supersonic flow within a convergent nozzle with a ramp test case. The modified limiter formulation is observed to perform better than the reference schemes, but unwanted oscillations can still develop in the solution, becoming more prominent with the increase of the order of the spatial discretization.

Keywords: Flux Limiter, High-Order Formulation, FR/CPR, Supersonic Flow

# 1. Introduction

Among the different types of numerical methods currently used to solve the gas dynamics equations, compact, high-order schemes have been identified over the past few decades to be particularly well suited for performing high-fidelity numerical simulations [1]. Due to the low dissipative nature of high-order schemes, aeroacoustic analysis and high-lift prediction are among the many aeronautical applications that benefit from their use. Furthermore, the compact stencil of these schemes allows for efficient parallel implementations on distributed memory computer architectures by reducing the amount of cross-node communication calls required to compute them. Essentially, all the required information exchange between computer nodes happens over a well-defined surface of the computational domain. This is in stark contrast to wide-stencil, high-order formulations, such as the essentially non-oscillatory (ENO) [2] and weighted essentially non-oscillatory (WENO) class of schemes [3], which may require the synchronization of many layers of ghost-cells, or similar constructs, in order to effectively implement them in massively parallel computer clusters.

When it comes to the simulation of compressible flows in the presence of shock waves, however, a major shortcoming of compact, high-order schemes becomes apparent. Similar to what happens to other types of numerical methods, compact, high-order schemes are susceptible to the development of spurious oscillations in regions near discontinuities, such as shock waves [4, 5]. In order to avoid such behavior, general shock-capturing schemes adopt one of two different strategies. The first one is the explicit addition of artificial dissipation terms to the original equations. In the present context, a well-known approach was introduced by Persson and Peraire in Ref. [6], which included not only an artificial dissipation model, but also a sensor for the detection of solution discontinuities. The second approach is to employ a limiter formulation which, together with a discontinuity sensor, should decrease the high-order scheme to a highly dissipative, first-order formulation, effectively reducing the spurious oscillations. For high-order schemes applied to unstructured meshes, examples of such

limiter formulations were introduced by Michalak and Ollivier-Gooch in Ref. [7], as well as by Li and Wang in Ref. [8]. Yet, both strategies rely on the same underlying mechanism in order to keep the numerical solution oscillation-free. That is, additional numerical dissipation is added to the solution in regions that contain discontinuities.

Unfortunately, if the computational cells that contain a discontinuity carry any meaningful amounts of information that require a high-order formulation in order to correctly represent the local solution behavior, the introduction of additional numerical dissipation can be a destructive process. This effectively removes one of the main advantages of this class of schemes, which is their low dissipative nature. Recently, a new family of limiters has been proposed by Nishikawa [9], entitled the "R" family of limiters, which allows for the construction of limiter formulations whose dissipative properties are compatible with high-order schemes of arbitrary order. However, to the best of the authors' knowledge, practical numerical experiments with these schemes have been constrained to an edge-based numerical formulation [9] using the flux and solution reconstruction (FSR) high-order scheme [10]. Hence, it is important to assess the limiter behavior when used in conjunction with other compact, high-order schemes. The present effort is inserted exactly in this context, and focus on analyzing the numerical characteristics of three different limiters from the R family, namely the  $R_3$ ,  $R_4$  and  $R_5$ , when applied to the solution of the Euler equations in the presence of strong shock waves.

The current analysis uses the flux reconstruction / correction procedure via reconstruction (FR/CPR) framework [11, 12, 13, 14, 15] in order to develop unstructured, high-order numerical schemes for the solution of the Euler equations. This framework has been chosen due to its ability to recover other well-known, high-order schemes for the solution of hyperbolic equations, such as the discontinuous Galerkin (DG) [16] and the spectral difference (SD) [17, 18] methods, thus allowing for a broader analysis of the new limiters. An in-house implementation of the second-, third- and forth-order FR/CPR schemes [19], coupled with Roe's numerical flux [20] and the BDF1 implicit time-march [21], is used to solve supersonic flow problems of aeronautical interest. A two-dimensional, inviscid, supersonic flow within a convergent nozzle with a ramp case is used to assess the differences between each limiter formulation. In this test case, a strong shock wave is developed at the compression corner of the ramp, followed by a sequence of strong shock-wave reflections, thus creating a well-suited test case for assessing the performance of each limiter. Results obtained using a modified version of the Michalak and Ollivier-Gooch limiter [7], as proposed by Li and Wang [8], are also added to the analysis for comparison.

In the paper, the introduction section is followed by a presentation of the numerical formulation used in the present work. Then, a brief description of the test case is performed, followed by the obtained results. Finally, concluding remarks are presented.

# 2. Numerical Formulation

# 2.1 The FR/CPR Framework

In order to properly introduce the formulation of the three limiters, it is important to first briefly describe the FR/CPR framework [22]. Consider the following generic system of nonlinear, hyperbolic conservation laws written in the Cartesian coordinate system:

$$\frac{\partial \mathbf{Q}}{\partial t} + \vec{\nabla} \cdot \vec{\mathbf{\mathscr{F}}}(\mathbf{Q}) = 0 , \qquad (1)$$

where Q is a vector of conserved variables,  $\mathscr{F}$  is a nonlinear flux vector and t is the time variable. By dividing the computational domain into a finite number of non-overlaping cells, a suitable weak form of the above equation can be obtained by multiplying both of its members by an arbitrary test function, w(x, y, z), and then integrating the resulting equation over the i-th cell of volume  $\mathbb{V}$ , as follows

$$\int_{\mathbb{V}_{\cdot}} w \left( \frac{\partial \mathbf{Q}}{\partial t} + \vec{\nabla} \cdot \vec{\mathbf{F}} \right) d\mathbb{V} = 0 . \tag{2}$$

The overall solution to the above equation is approximated by a piecewise continuous function, where the solution is continuous inside each cell and discontinuous across its faces. In this particular formulation, the solution inside each cell is approximated by a polynomial,  $Q_i$ , that belongs to the space of

all polynomials of  $\kappa$ -degree or less,  $P^{\kappa}$ . Considering a nodal formulation, this polynomial can be fully described by a finite number of solution values evaluated at well-defined points located inside the cell, referred to as solution points (SPs), together with an appropriate set of Lagrange interpolating polynomials, which compose the basis of  $P^{\kappa}$ . The SPs are usually placed in the same location as a set of quadrature points, which enhances the overall numerical behavior of the scheme and also avoids the need for extra interpolations when performing certain operations. By applying Eq. (2) to the i-th cell, integrating by parts its second term, making use of the Gauss theorem, defining a common numerical flux across the cell interface,  $\mathscr{F}_k$ , and applying integration by parts once again, the following weak-form of Eq. (1) is obtained

$$\int_{\mathbb{V}_{i}} w \frac{\partial \mathbf{Q}_{i}}{\partial t} d\mathbb{V} + \int_{\mathbb{V}_{i}} w \left( \vec{\nabla} \cdot \vec{\mathscr{F}}_{i} \right) d\mathbb{V} + \oint_{\mathbb{S}_{i}} w \left[ \mathscr{F}_{k} - \vec{\mathscr{F}}_{i} \cdot \hat{n}_{k} \right] d\mathbb{S} = 0 . \tag{3}$$

In Eq. (3),  $\mathbb{S}_i$  is the boundary surface of the current cell, i.e., the union of its faces, and  $\vec{\mathscr{F}}_i \equiv \vec{\mathscr{F}}(\boldsymbol{Q}_i)$ . The common discrete fluxes across cell interfaces are defined at another set of points, referred to as flux points (FP), which are located at the cell boundaries and are typically computed by employing a numerical flux definition, such as a Riemann solver or similar construct. In the present effort, the authors have chosen to use Roe's numerical flux [20], which assumes the following form when evaluated at the k-th flux point

$$\mathscr{F}_k = \mathscr{F}_{Roe_k}(\mathbf{Q}_k^+, \mathbf{Q}_k^-, \hat{n}_k)$$
, (4)

where  $\hat{n}_k$  is the outward-pointing, face unitary normal vector, evaluated at the k-th FP, while  $\mathbf{Q}_k^+$  and  $\mathbf{Q}_k^-$  are the reconstructed conserved variable values evaluated immediately to the left and right sides of the current interface k-th FP. Similarly to solution points, flux points are also typically located at quadrature locations for improved robustness and computational efficiency. The last term of Eq. (3) is essentially a correction term, that measures the difference between the common numerical flux,  $\mathscr{F}_k$ , and the internal, continuous flux across the cell interface,  $\vec{\mathscr{F}}_i \cdot \hat{n}_k$ . By defining  $[\mathscr{F}]_k \equiv \mathscr{F}_k - \vec{\mathscr{F}}_i \cdot \hat{n}_k$ , the surface integral can be cast into a volume integral by a collocation-like procedure [13]

$$\oint_{\mathbb{S}_i} w[\mathscr{F}]_k d\mathbb{S} = \int_{\mathbb{V}_i} w \delta_i d\mathbb{V} , \qquad (5)$$

where  $\delta_i$  is the FR/CPR correction function. Substituting Eq. (5) in Eq. (3) and remembering that the weak form should be true for all w, the corrected, discrete form of the original conservation laws is obtained

$$\frac{\partial \mathbf{Q}_i}{\partial t} + \vec{\nabla} \cdot \vec{\mathscr{F}}_i + \mathbf{\delta}_i = 0 \ . \tag{6}$$

In general, the flux vector is a non-polynomial function of  $Q_i$ . As such, it is necessary to project it into  $P^{\kappa}$  in order to allow its divergent to be computed efficiently. Thus, the above equation, when evaluated at the j-th SP of the current i-ith cell, becomes

$$\frac{\partial \mathbf{Q}_{i,j}}{\partial t} + \prod_{j} \left( \vec{\nabla} \cdot \vec{\mathscr{F}}_{i} \right) + \mathbf{\delta}_{i,j} = 0 , \qquad (7)$$

where the second term is the projection of the flux divergent on  $P^{\kappa}$ , evaluated at the j-th SP. Here, it is computed by evaluating the flux vectors at each SP, interpolating them using the current Lagrange polynomial basis and then analytically computing the divergent of the resulting function. Equation (7) is the final form of the FR/CPR scheme applied to a system of hyperbolic conservation laws. Furthermore, in this particular implementation, Eq. (7) is time-integrated by using the BDF1 (implicit Euler) first-order scheme, which is well suited for the present application since only the steady-state solution is desired, coupled with a Newton-Krylov type solver [23].

# 2.2 High-Order Limiter Formulation

The limiter formulation acts directly over the solution reconstruction inside a cell. If  $q_i$  is a generic, scalar conserved variable evaluated at the *i*-th cell, then by defining  $q_{HO_i}$  as the high-order polynomial representation of  $q_i$  in the absence of a limiter, the limited reconstruction becomes

$$q_i = \overline{q}_i + \phi_i \left( q_{HO_i} - \overline{q}_i \right) \tag{8}$$

in which the overbar indicates average cell values and  $\phi_i$  is the limiter value associated with the *i*-th cell. From Eq. (8), it becomes clear that if the reconstruction is fully limited, that is  $\phi_i = 0$ , then the overall solution becomes piecewise constant in the affected regions, thus decreasing the scheme to first-order in terms of spatial discretization accuracy.

Nishikawa's  $R_3$ ,  $R_4$  and  $R_5$  limiters, referred here as  $\phi^{R_3}$ ,  $\phi^{R_4}$  and  $\phi^{R_5}$ , respectively, are first evaluated at each FP using the following equations applied to each one of the conserved variables

$$\Delta_{-} \equiv q_{HO_{i,i}} - \overline{q}_i , \qquad (9)$$

$$\Delta_{+} \equiv \begin{cases} \overline{q}_{\text{max}} - \overline{q}_{i}, & \text{if } q_{\text{HO}_{i,j}} \geq \overline{q}_{i}, \\ \overline{q}_{\text{min}} - \overline{q}_{i}, & \text{if } q_{\text{HO}_{i,j}} < \overline{q}_{i}, \end{cases}$$

$$\tag{10}$$

$$\phi_{i,j}^{R_p} = \begin{cases} \frac{(a^p + \varepsilon^p) + aS_p}{(a^p + \varepsilon^p) + b\left(\Delta_+^{p-1} + S_p\right)}, & \text{if } a \le 2b, \\ 1, & \text{if } a > 2b, \end{cases}$$

$$\tag{11}$$

where p = 3, 4, 5 and

$$S_3 = 4b^2$$
, (12)

$$S_4 = 2b \left[ a^2 - 2b \left( a - 2b \right) \right] ,$$
 (13)

$$S_5 = 8b^2 \left[ a^2 - 2b \left( a - b \right) \right] ,$$
 (14)

with

$$a \equiv |\Delta_+| \quad , \tag{15}$$

$$b \equiv |\Delta_-| \ , \tag{16}$$

$$\varepsilon^p = (K\Delta x_i)^{p+1} \ . \tag{17}$$

In the limiter formulation,  $\overline{q}_{\max}$  and  $\overline{q}_{\min}$  are the maximum and minimum cell-averaged conserved variable values among the current cell and all of its face-sharing neighbors. Furthermore,  $\Delta x_i$  is a characteristic length of the cell, which here is taken as  $\Delta x_i = \mathbb{V}_i^{\frac{1}{3}}$ . Finally, K is a control constant that allows the scheme to achieve better convergence properties, with values typically taken to be within the interval  $K \in [0.01, 10]$ , provided the equations being solved are properly made dimensionless. The actual cell limiter is simply the minimum value among those computed at each flux point of the current cell. That is

$$\phi_i^{R_p} = \min\left(\phi_{i,j}^{R_p}\right). \tag{18}$$

Ideally, the  $R_3$  limiter should be able to keep the truncation error of the limited scheme compatible with a third-order formulation. Similar interpretation is also true for the  $R_4$  and  $R_5$  limiters, which should be compatible with forth and fifth-order formulations, respectively.

In the present work, the aforementioned limiter is compared with the well-known Michalak and Ollivier-Gooch limiter [7], but with the smoothing process performed by employing Persson and

Peraire discontinuity sensor [6], as described by Li and Wang in Ref. [8]. For completeness, this limiter formulation, referred here as  $\phi^S$ , is also described.

Similar to what has been previously done, first  $\phi^S$  is evaluated at each FP of the *i*-th cell using the function below [7, 8]

$$\phi_{i,j}^S = \begin{cases} -\frac{4}{27} \left(\frac{\Delta_+}{\Delta_-}\right)^3 + \frac{\Delta_+}{\Delta_-} & \text{, if } \frac{\Delta_+}{\Delta_-} < 1.5, \\ 1 & \text{, otherwise.} \end{cases}$$

$$\tag{19}$$

In situations in which the term  $\Delta_+/\Delta_-$  would result in a division by zero, it is made equal to 1. A preliminary cell value for the limiter can, then, be computed by using the following expression

$$\tilde{\phi}_i^S = \min\left(\phi_{i,j}^S\right). \tag{20}$$

In order to avoid the possible effects that the limiter can have on uniform regions of the solution and near smooth extrema, a smoothness indicator,  $S_i$ , associated with the current i-cell is introduced [6, 8]

$$S_i = \log_{10} \left( \frac{\langle q_i - \hat{q}_i, q_i - \hat{q}_i \rangle_i}{\langle q_i, q_i \rangle_i} \right) , \tag{21}$$

in which  $\langle \cdot, \cdot \rangle_i$  is the standard polynomial inner product applied to the *i*-th cell. The term  $\hat{q}_i$  is the orthogonal projection of  $q_i$  on  $P^{\kappa-1}$ . In regions in which the solution would be oscillatory, such as near discontinuities, the numerator of Eq. (21) is expected to become large. In contrast, smooth regions of the flow should not result in such large values, therefore allowing discontinuities to be identified. Next,  $S_i$  is rescaled to lie in the [0,1] interval by computing

$$\sigma_{i} = \begin{cases} 1 & \text{, if } S_{i} \leq S_{0} - \omega \text{,} \\ \frac{1}{2} \left[ 1 - \sin \left( \frac{\pi(S_{i} - S_{0})}{2\omega} \right) \right] & \text{, if } S_{0} - \omega < S_{i} < S_{0} + \omega \text{,} \\ 0 & \text{, if } S_{i} \geq S_{0} + \omega \text{.} \end{cases}$$

$$(22)$$

In this implementation,  $S_0$  and  $\omega$  are constants and equal to -3.7 and 1.0, respectively. Finally, a linear blend between  $\tilde{\phi}_i^S$  and a constant function equal to 1 is performed using  $\sigma_i$ , thus allowing the cell limiter value to be computed

$$\phi_i^S = \sigma_i + (1 - \sigma_i)\tilde{\phi}_i^S. \tag{23}$$

It is important to emphasize that the limiter value is computed for each one of the conserved variables, separately.

The authors observed that the introduction of this particular smoothness indicator can substantially improve the quality of the results. Therefore, a modified version of the  $\phi^{R_p}$  limiters is also considered here, called  $\phi^{R_pS}$ , in which the same process defined by Eqs. (21) and (22) is performed, allowing  $\phi^{R_pS}$  to be defined as

$$\phi_i^{R_pS} = \sigma_i + (1 - \sigma_i)\phi_i^{R_p}, \qquad (24)$$

for, once again, p equal to 3, 4 and 5. Since the introduction of the  $\varepsilon^p$  term in Eq. (11) aims to address the same problem tackled by the smoothness indicator, there is no need to use it when computing  $\phi_i^{R_p}$  in Eq. (24). Hence, the limiter value used in the right-hand side of Eq. (24) is computed using a constant  $\varepsilon^p$  value equal to  $10^{-25}$ , employed exclusively to avoid a division by zero.

# 3. Test Case Setup and Results

The test case considered in this paper is a two-dimensional, supersonic flow in a convergent nozzle with a ramp [7, 8]. The domain is modeled as a channel with an included 15 deg. compression ramp, followed by a 15 deg. expansion corner. The domain is extended further on both the upstream and downstream directions in relation to the ramp in order to allow the development of the flowfield and avoid possible numerical problems, as shown in Fig. 1. To better highlight the diffusive properties of each scheme, a single coarse mesh consisting of  $96 \times 32$  quadrilateral cells is considered, as also

shown in Fig. 1. The left boundary is taken to be a supersonic inlet, in which atmospheric air enters the domain perpendicular to the boundary surface with a Mach number  $M_{\infty} = 2.0$ . The right boundary is a supersonic outlet, the bottom boundary is an inviscid wall and the top one is a symmetry plane.

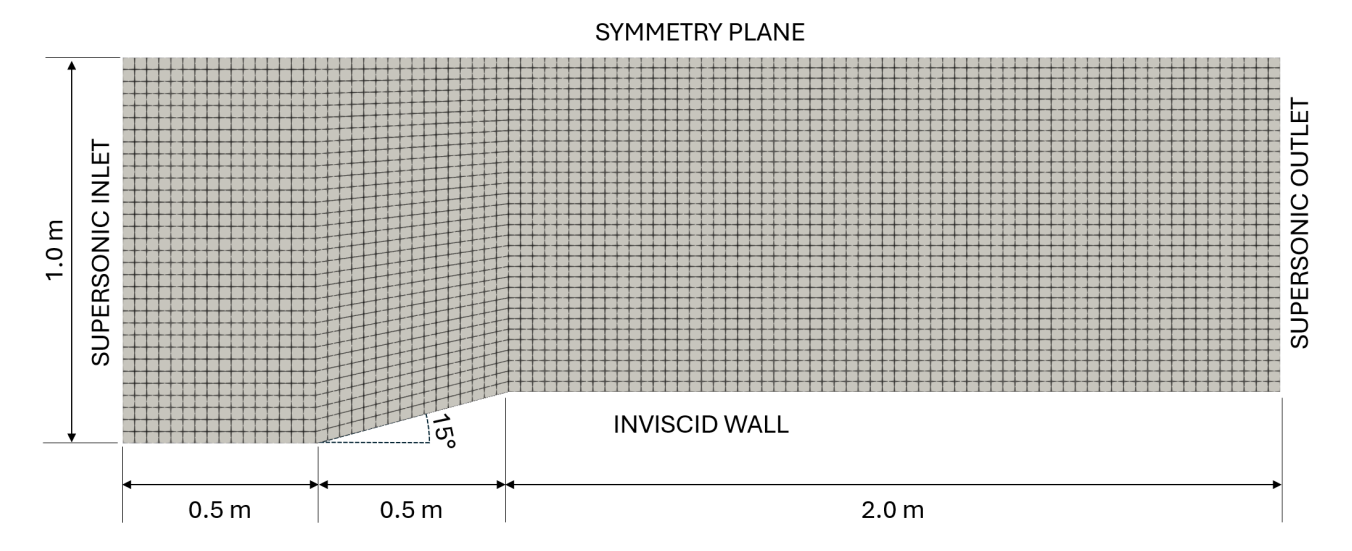


Figure 1 – Computational domain for the two-dimensional, supersonic flow in a convergent nozzle with a ramp test case.

First, the original  $\phi^{R_p}$  limiters are compared to their smoothed counterparts,  $\phi^{R_pS}$ . Figure 2 shows the steady-state contour plots of the limiter value, with respect to the total energy per unit of volume, computed using  $\phi^{R_p}$  and  $\phi^{R_pS}$  with a fourth-order FR/CPR scheme  $(P^3)$ . Values related to  $\phi^{R_p}$  were computed by taking K=5, which was found by the authors to be a good compromise between avoiding limiter activation in smooth regions of the flow and keeping a reasonably oscillation-free solution. In the present implementation, no formal convergence of the steady-state residue to machine zero is obtained with any of the limiters considered here. Still, macro-properties of the solution, such as the aerodynamic forces that act upon the inviscid wall boundary, do fully converge, exhibiting a similar behavior to the one described in Ref. [8].

From Fig. 2, it becomes immediately clear that the results associated with  $\phi^{R_pS}$  assume values different from 1 in regions of the domain which are better aligned with the expected location of the shock wave. In contrast, limiter values computed using the three  $\phi^{R_p}$  limiters are prone to develop seemingly random perturbations, particularly near the outflow boundary. As designed, none of the limiters exhibit any type of spurious activations in the freestream region of the flow, located between the inflow boundary and the first shock front. All limiters appear to be particularly sensitive to the region near the expansion corner, where an expansion fan develops. However, except for the cells that are located directly adjacent to the wall, limiter values obtained by employing all three  $\phi^{R_pS}$  formulations, when evaluated at the expansion fan region, always assume values that are higher than 0.6. On the other hand, values computed using any of the three  $\phi^{R_p}$  limiters are seen to become as low as 0.3 in the same region.

Another important solution feature to consider lies in the region between the first and the second shock reflection, near the symmetry plane. There, it is possible to observe a horizontal and a vertical region in which all limiters wrongly deviate from 1. The horizontal line spans a single cell in its width direction, and probably originates from small perturbations that arise from the interaction between the first incident shock and the symmetry plane, where all limiters assume a value that is virtually zero, and then get advected throughout the domain. The vertical line spans two cells in its width direction and is particularly critical in the results shown for the  $\phi^{R_p}$  limiters, since the scheme decays completely to a piecewise constant solution representation, thus becoming first-order accurate. From the limiter values alone it is already possible to assess the improvements achieved by the introduction of a smoothness indicator to the original  $\phi^{R_p}$  limiter formulation.

To better visualize the impact that the limiter values shown in Fig. 2 have on the actual property values, Mach number contour plots related to the same solution are shown in Fig. 3. In an effort to

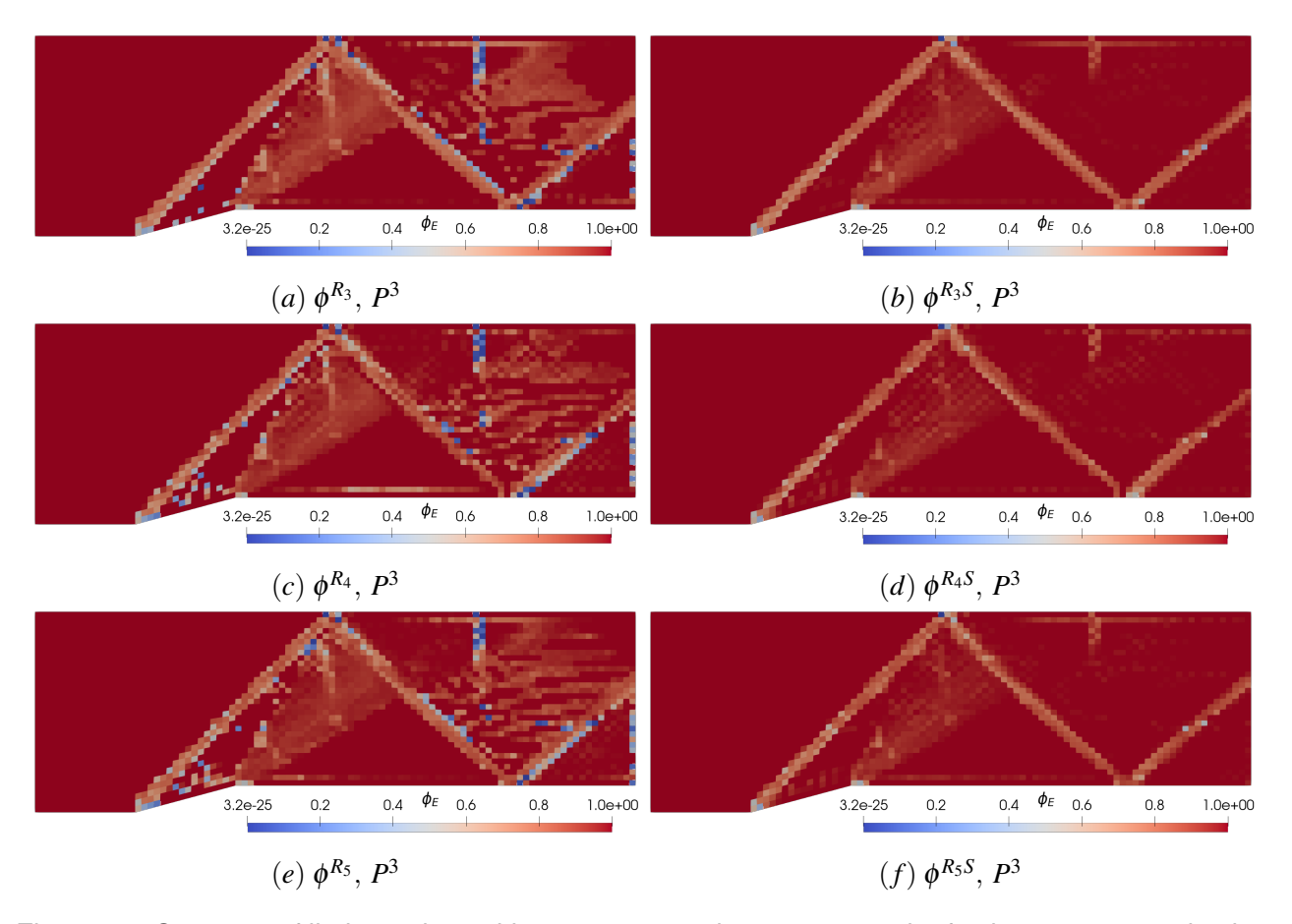


Figure 2 – Contours of limiter value, with respect to total energy per unit of volume, computed using different limiter formulations with a fourth-order FR/CPR scheme ( $P^3$ ).

improve the readability of the data, the contour colors have been discretized in 20 different zones. The main features of this inviscid flow appear to be well represented by all schemes. In particular, the shock width is apparently fully contained within a single cell, although the shock surface itself is not particularly well-defined due to the lack of resolution from the usage of a coarse mesh. It is also promptly noticed that all solutions, which are supposed to be monotonic, are not free of oscillations. Small oscillations can be seen in the expansion fan region, as well as in between the two shock reflections. The misalignment between the shock surface and mesh lines, coupled with the usage of a high-order, low-dissipation scheme, is a possible source of this problem.

Figure 4 shows the Mach number values evaluated along a reference horizontal line that is located 0.5 m away from the symmetry plane. For this particular plot, the internal solution polynomial of each cell is fully represented. The oscillatory behavior is evident, but the overall shape of the solution appears to agree well with each other. Based on the Mach number values achieved in the regions that surround the shock waves, the  $R_4$  formulations, both the original and the smoothed one, appear to be less dissipative than the  $R_3$ , as expected, and perform as good as the  $R_5$ . Since this solution is constrained to a  $P^3$  polynomial space, the scheme is, at best, forth-order accurate and, thus, should not be able to achieve sufficiently low amounts of artificial dissipation to allow the differences between the  $R_4$  and  $R_5$  schemes to be visualized. Furthermore, when comparing the original formulations with their smoothed counterparts, it is also possible to see that the smoothed ones do indeed lead to a less dissipative solution, evidenced by the higher peak values in the regions that surround the discontinuities.

It must be emphasized, though, that the oscillations are primarily visible due to the high-order representation of the solution. By construction, the limiter formulations described in this work can only guarantee that no local new extremum will be created with respect to the cell-averaged values of the current cell and its direct neighbors. No restriction is imposed on the local values of the solution polynomial, which leads to the oscillatory behavior described here. If cell-averaged property values

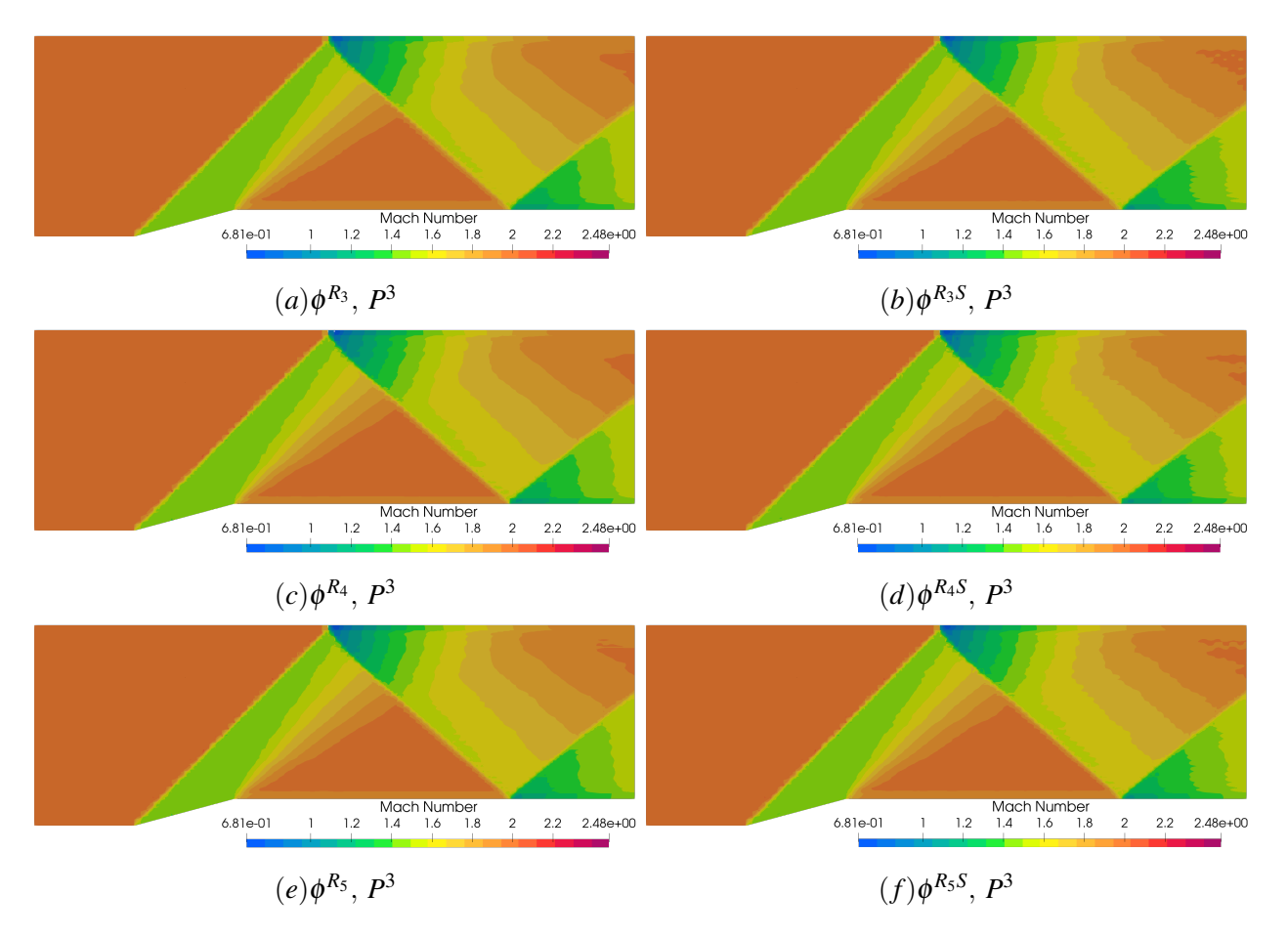


Figure 3 – Mach number contours computed using different limiter formulations with a fourth-order FR/CPR scheme.

are plotted instead of the high-order polynomial representation, the oscillations disappear completely, as shown in Fig. 5. Nevertheless, the same conclusion regarding the relative performance of each limiter continues to be valid.

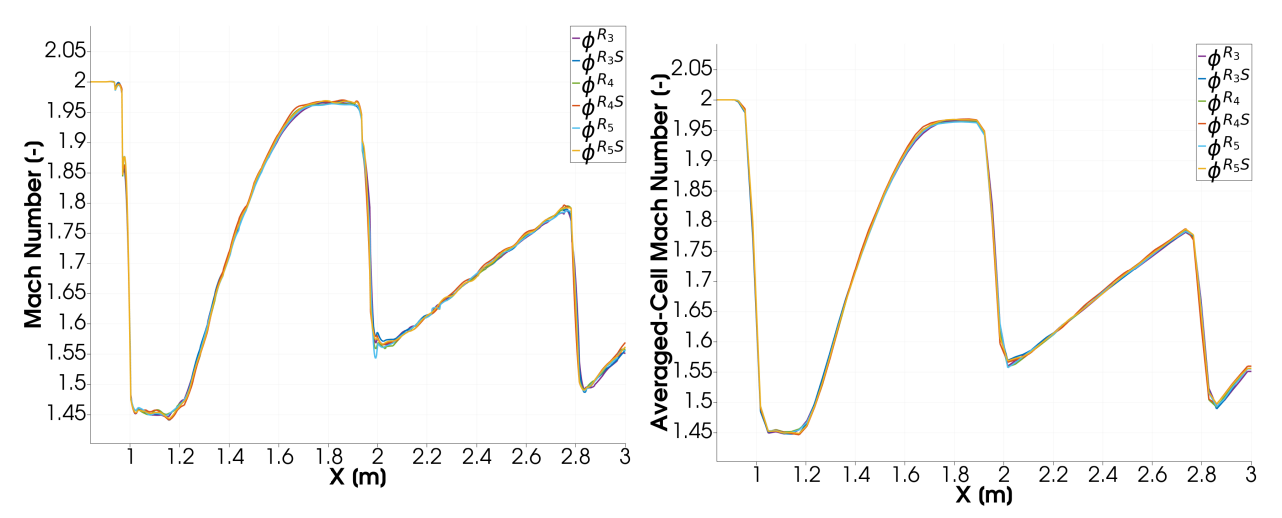


Figure 4 – High-order plot of the solution Mach number evaluated along the horizontal reference line computed using a 4th-order FR/CPR scheme.

Figure 5 – Averaged-cell Mach number value evaluated along the horizontal reference line computed using a 4th-order FR/CPR scheme.

Since coupling the original  $\phi^{R_p}$  limiters with a smoothness indicator seems to produce better results for the particular case being studied here, from now on the R family of limiters is only considered

in its  $\phi^{R_pS}$  form. Figure 6 displays limiter values, with respect to density, computed using the  $\phi^{R_pS}$  and  $\phi^S$  limiters with second-, third- and fourth-order FR/CPR schemes, *i.e.*, with  $P^1$ ,  $P^2$  and  $P^3$ , respectively. From a qualitative perspective, the results shown in Fig. 6 can be considered reasonably "well-behaved", but far from ideal. All limiters seem to deviate from 1 near the shock-wave, as they should, close to the expansion fan and in the horizontal and vertical lines located between the first and second shock reflections, near the symmetry plane, as previously discussed. Results obtained with the second-order scheme display a more consistent limiter value distribution. In particular, the data shown for the second-order formulation with the  $\phi^S$  limiter does not show any sensitivity to the horizontal and vertical line regions, deviating from the unitary value only when directly adjacent to the shock-waves and close to the geometrical discontinuity defined by the expansion corner. Another trend evident from these data is that lower-order schemes tend to result in overall lower limiter values. Therefore, they more quickly restrict the solution polynomial representation inside a cell when compared to the same limiters used in conjunction with discretization schemes of higher order. This is an intended behavior, as it helps to maintain a low-level of artificial dissipation that is compatible with a high-order formulation.

Lastly, pressure values evaluated along the horizontal reference line, located 0.5 m away from the symmetry plane, are shown for  $\phi^{R_pS}$  and  $\phi^S$  in Fig. 7, including the high-order polynomial representation, and in Fig. 8, including cell-averaged values. Results shown in Figs. 7 and 8 were computed using second-, third- and fourth-order FR/CPR schemes. In regard to the cell-averaged data, the overall tendency of all schemes to converge to the same solution as the order is increased is clearly displayed, leading to well-defined peaks and valleys and demonstrating that the formulations employed are consistent. However, no major differences can be spotted between the results when the analysis is constrained to cell-average data only. When the high-order representation is taken into account, as shown in Fig. 7, that ceases to be the case. Calculations that use a  $P^1$  reconstruction are particularly prone to create undershoots in the solution in regions located right upstream of the shock, particularly before the second shock reflection. This effect gets less pronounced when the order of the scheme is increased. Other types of oscillations, despite being small in amplitude, also become increasingly more pronounced in regions where the flow is supposed to be free of significant property gradients as the order of the discretization scheme increases. Despite being oscillatory, the high-order representation of the solution permits a more precise assessment of the quality of the limiter formulations. By taking the pressure peak located right after the first shock reflection as a reference for the dissipative properties of each limiter, it is possible to state that all three  $\phi^{R_pS}$  limiters are able to capture a more well-defined, less-diffused, peak, especially when third- and forth-order discretization schemes are used. The difference is small for this particular case, but still measurable. Since the difference in computational cost between any of the  $\phi^{R_pS}$  limiters and the  $\phi^S$  limiter is negligible, it is possible to conclude that, out of all the limiter formulations herein considered, it is overall a better option to employ a limiter from the  $\phi^{R_pS}$  family when simulating cases that are similar to the one studied in this paper using higher than second-order schemes.

# 4. Concluding Remarks

The present paper assessed the quality of the flow solutions obtained by using the *R* family of limiters, when compared with calculations that used the well-known Michalak and Ollivier-Gooch limiter. The limiters were implemented in the context of a compact, high-order discretization scheme. Two versions were considered for each limiter, namely, the original, unmodified formulation as stated in the literature, as well as a modified formulation, in which the original limiter is augmented by using a smoothness indicator function. The entire analysis was constrained to a single supersonic flow in a convergent nozzle with a ramp test case. The current results show that coupling the original *R* limiters with a smoothing function can significantly improve the behavior of those limiters, especially by decreasing the size of the regions in which they incorrectly decay the order of the scheme without any real need for it. Even in the presence of a smoothing function, however, the limiter behavior is not free from imperfections, and can be observed to degrade the quality of the solution even in smooth regions of the flow. When compared to the Michalak and Ollivier-Gooch limiter, the modified *R* limiters displayed an overall similar behavior in smooth regions of the flow, but was seen to be able to better define the solution peaks and valleys that surround a discontinuity. Since the computational cost of

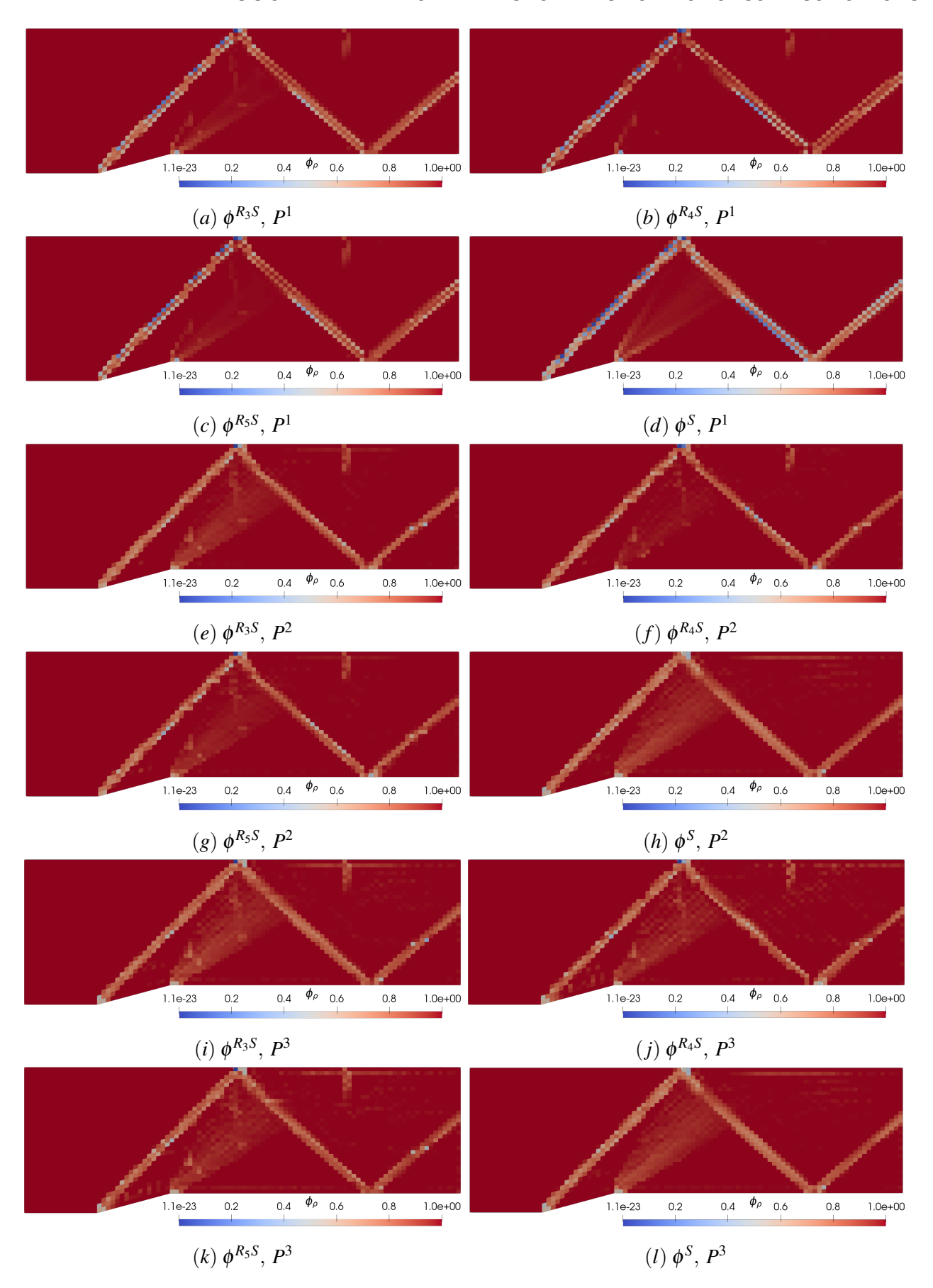


Figure 6 – Contours of limiter value, with respect to density, computed using different limiter formulations and FR/CPR orders.

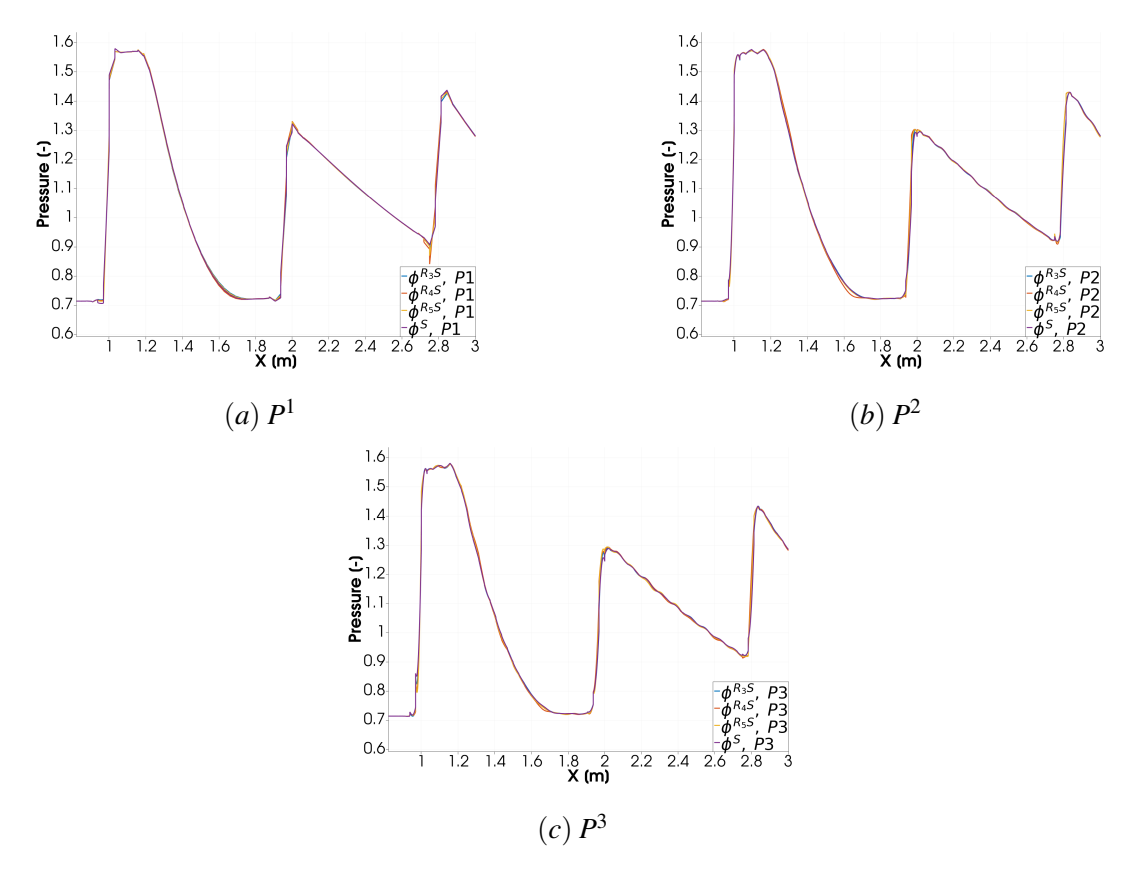


Figure 7 – High-order plot of pressure values evaluated along the horizontal reference line computed using  $P^1$ ,  $P^2$  and  $P^3$  FR/CPR schemes.

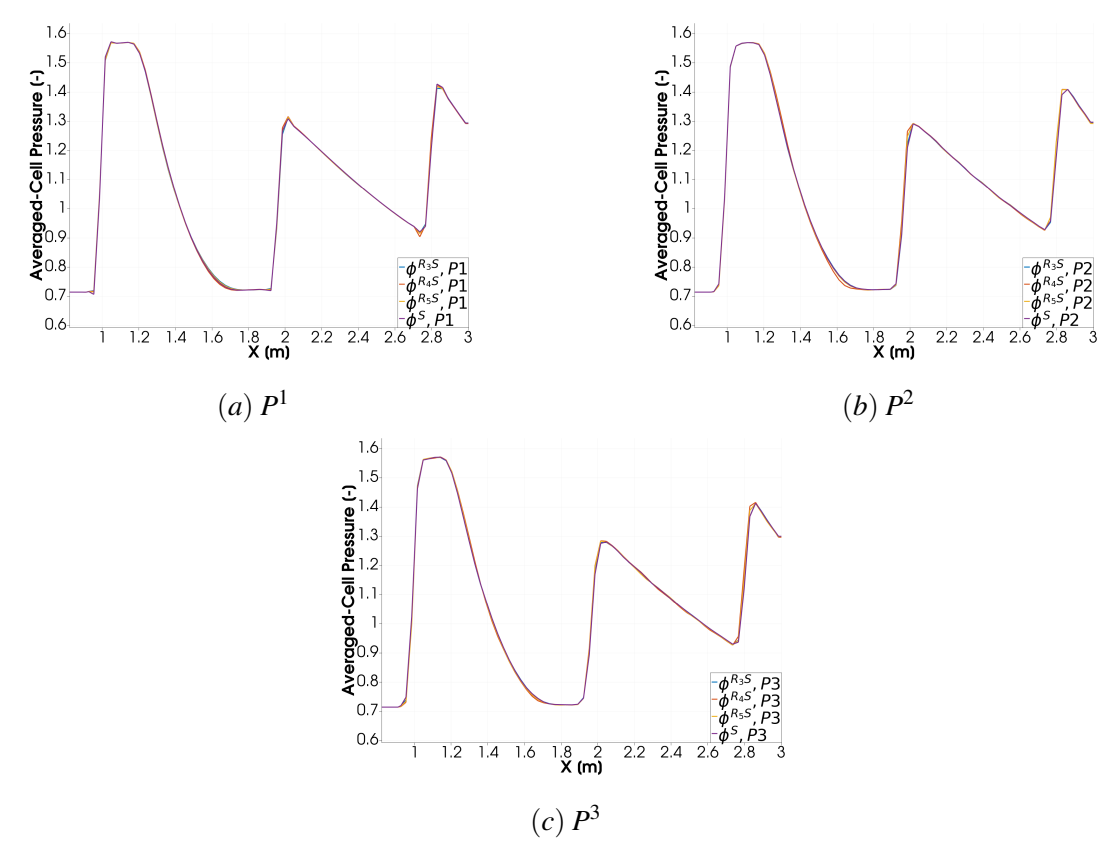


Figure 8 – Averaged-cell pressure value evaluated along the horizontal reference line computed using  $P^1$ ,  $P^2$  and  $P^3$  FR/CPR schemes.

the modified R limiter is very similar to the Michalak and Ollivier-Gooch limiter, in situations involving flows similar to the one studied here, employing a suitable limiter from the  $\phi^{R_pS}$  family appears to be the overall best choice in compact, high-order applications.

# 5. Acknowledgments

The authors wish to express their gratitude to Fundação de Amparo à Pesquisa do Estado de São Paulo, FAPESP, which has supported the present research under the Research Grants No. 2013/07375-0, No. 2021/00147-8 and No. 2023/08573-1. The authors also gratefully acknowledge the support for the present research provided by Conselho Nacional de Desenvolvimento Científico e Tecnológico, CNPq, under the Research Grant No. 315411/2023-6. The work has taken advantage of the availability of the computational resources of the Center for Mathematical Sciences Applied to Industry, CeMEAI, also funded by FAPESP under the Research Grant No. 2013/07375-0.

## 6. Contact Author Email Address

Frederico Bolsoni Oliveira: fredericobolsoni@gmail.com João Luiz F. Azevedo: joaoluiz.azevedo@gmail.com

Z. J. Wang: zjw@ku.edu

# 7. Copyright Statement

The authors confirm that they, and/or their company or organization, hold copyright on all of the original material included in this paper. The authors also confirm that they have obtained permission, from the copyright holder of any third party material included in this paper, to publish it as part of their paper. The authors confirm that they give permission, or have obtained permission from the copyright holder of this paper, for the publication and distribution of this paper as part of the ICAS proceedings or as individual off-prints from the proceedings.

## References

- [1] Wang, Z. J. et. al., "High-Order CFD Methods: Current Status and Perspective," *International Journal for Numerical Methods in Fluids*, Vol. 43, 2012, pp. 1–42.
- [2] Harten, A., Osher, S., Engquist, B., and Chakravarthy, S. R., "Uniformly High-Order Accurate Essentially Non-Oscillatory Schemes III," *Journal of Computational Physics*, Vol. 71, No. 2, 1987, pp. 231–303.
- [3] Liu, X. D., Osher, S., and Chan, T., "Weighted Essentially Non-Oscillatory Schemes," *Journal of Computational Physics*, Vol. 115, No. 1, 1994, pp. 200–212.
- [4] Oliveira, F. B. and Azevedo, J. L. F., "Effects of Numerical Parameters and Artificial Dissipation in the Simulation of Inviscid Nozzle Flows," COBEM Paper No. 2019-1227, 25th ABCM International Congress of Mechanical Engineering, Uberlândia, Brazil, 2019.
- [5] Oliveira, F. B. and Azevedo, J. L. F., "Effects of Numerical Parameters in the Simulation of Supersonic Blunt Body Flows," ENCIT Paper No. 2020-0300, 18th Brazilian Congress of Thermal Sciences and Engineering, Online, Nov. 2020.
- [6] Persson, P.-O. and Peraire, J., "Sub-Cell Shock Capturing for Discontinuous Galerkin Methods," AIAA Paper No. 2006-112, *44th AIAA Aerospace Sciences Meeting and Exhibit*, Reno, Nevada, USA, Jan. 2016.
- [7] Michalak, K. and Ollivier-Gooch, C. F., "Limiters for Unstructured Higher-Order Accurate Solutions of the Euler Equations," AIAA Paper No. 2008-776, 46th AIAA Aerospace Sciences Meeting and Exhibit", Reno, Nevada, USA, Jan. 2008.
- [8] Li, Y. and Wang, Z. J., "Recent Progress in Developing a Convergent and Accuracy Preserving Limiter for the FR/CPR Method," AIAA Paper No. 2017-0756, *55th AIAA Aerospace Sciences Meeting*, Grapevine, Texas, USA, Jan. 2017.
- [9] Nishikawa, H., "New Unstructured-Grid Limiter Functions," AIAA Paper No. 2022-1473, AIAA SciTech 2022 Forum, San Diego, CA & Virtual, Jan. 2022.
- [10] Nishikawa, H., "Economically High-Order Unstructured-Grid Methods: Clarification and Efficient FSR Schemes," *International Journal for Numerical Methods in Fluids*, Vol. 93, No. 11, 2021.
- [11] Huynh, H. T., "A Flux Reconstruction Approach to High-Order Schemes Including Discontinuous Galerkin Methods," AIAA Paper No. 2007-4079, 18th AIAA Computational Fluid Dynamics Conference, Miami, FL, USA, June 2007.

- [12] Huynh, H. T., "A Reconstruction Approach to High-Order Schemes Including Discontinuous Galerkin for Diffusion," AIAA Paper No. 2009-403, 47th AIAA Aerospace Sciences Meeting Including The New Horizons Forum and Aerospace Exposition, Orlando, FL, USA, Jan. 2009.
- [13] Wang, Z. and Gao, H., "A Unifying Lifting Collocation Penalty Formulation Including the Discontinuous Galerkin, Spectral Volume/Difference Methods for Conservation Laws on Mixed Grids," *Journal of Computational Physics*, Vol. 228, No. 21, 2009, pp. 8161–8186.
- [14] Huynh, H. T., Wang, Z. J., and Vincent, P. E., "High-Order Methods for Computational Fluid Dynamics: A Brief Review of Compact Differential Formulation on Unstructured Grids," *Computers & Fluids*, Vol. 98, 2014, pp. 209–220.
- [15] Wang, Z. J. and Huynh, H. T., "A Review of Flux Reconstruction or Correction Procedure via Reconstruction Method for the Navier-Stokes Equations," *Mechanical Engineering Reviews*, Vol. 3, No. 1, 2016.
- [16] Bassi, F. and Rebay, S., "A High-Order Accurate Discontinuous Finite Element Method for the Numerical Solution of the Compressible Navier-Stokes Equations," *Journal of Computational Physics*, Vol. 131, No. 2, 1997, pp. 267–279.
- [17] Liu, Y., Vinokur, M., and Wang, Z., "Spectral Difference Method for Unstructured Grids I: Basic Formulation," *Journal of Computational Physics*, Vol. 216, No. 2, 2006, pp. 780–801.
- [18] Liu, Y., Vinokur, M., and Wang, Z. J., "Discontinuous Spectral Difference Method for Conservation Laws on Unstructured Grids," *Computational Fluid Dynamics 2004*, edited by C. Groth and D. W. Zingg, Springer Berlin Heidelberg, Berlin, Heidelberg, 2006, pp. 449–454.
- [19] Wang, Z. J., "Wall-Modeled Large Eddy Simulation of the NASA CRM High-Lift Configuration with the High-Order FR/CPR Method," AIAA Paper No. 2022-3395, *AIAA AVIATION 2022 Forum*, Chicago, IL, Virtual, June 2022.
- [20] Roe, P. L., "Approximate Riemann Solvers, Parameter Vectors and Difference Schemes," *Journal of Computational Physics*, Vol. 43, No. 2, 1981, pp. 357–372.
- [21] Hirsch, C., Numerical Computation of Internal and External Flows Volume 1: Fundamentals of Numerical Discretization, Wiley, Chichester, 1st ed., 1988, p. 515.
- [22] Wang, Z. J., "Towards Wall-Resolved Large Eddy Simulation of the High-Lift Common Research Model with a High-Order Method," AIAA Paper No. 2023-2121, *AIAA SCITECH 2023 Forum*, National Harbor, MD, Jan. 2023.
- [23] de Araujo Jorge Filho, E. J. and Wang, Z. J., "A Matrix-free GMRES Algorithm on GPU Clusters for Implicit Large Eddy Simulation," AIAA Paper No. 2021-1837, *AIAA Scitech 2021 Forum*, Online, 2021.